ELSEVIER

Soil Dynamics and Earthquake Engineering 27 (2007) 564–576

SOIL DYNAMICS AND EARTHQUAKE ENGINEERING

www.elsevier.com/locate/soildyn

Earthquake damage detection in the Imperial County Services Building I: The data and time–frequency analysis

Maria I. Todorovska*, Mihailo D. Trifunac

Department of Civil Engineering, University of Southern California, Los Angeles, CA 90089-2531, USA

Received 3 March 2006; received in revised form 23 October 2006; accepted 24 October 2006

Abstract

The former Imperial County Services Building was a six-story reinforced concrete structure in the El Centro, California, severely damaged by the 1979 Imperial Valley earthquake. It represents a rare case of an instrumented building that has been damaged, and thus can serve as a full-scale benchmark to evaluate and further develop structural health monitoring methods. This paper presents an analysis of inter-story drifts, and of changes in the first NS and EW system frequencies (estimated from the ridge of the Gabor transform of the relative roof displacement response) as indicators of the occurrence of damage. The detected initial decreases of system frequency, of about 28% for NS and 24% for EW motions, are not believed to be due to severe damage. The subsequent decreases, of about 44% for NS and 21% for EW motions, are attributed to damage. Near the end of shaking, increases of about 35% for the NS and 36% for EW motions were detected. (These percentage changes were computed with respect to the *previous* value for particular interval, rather than a fixed reference). During the most severe shaking, the inter-story drifts exceeded 0.5% for NS and 1.5% for EW motions.

Keywords: Damage detection; Seismic monitoring; Structural health monitoring; Frequency response; Vibration; Earthquake response; Imperial County Services building; Earthquakes; Seismic surveys; Structural response; Building frequency

1. Introduction

One of the significant potential uses of data recorded by seismic arrays installed in structures is monitoring the health of the structure, to detect damage as it occurs, and issue an early warning after the earthquake, before physical inspection is possible. This requires structural health monitoring methods that are sufficiently sensitive, and robust when applied to real earthquake response data. The currently available vibration methods that use data from such arrays can determine if the structure has been damaged, but cannot indicate precisely the location of the damage, and are hence referred to as global. Most vibration based methods monitor changes in the *modal* properties of the structures (modal frequencies and mode shapes). The difficulties associated with these methods include: (i) the presence of other factors than damage that produce similar effects on the monitored parameters, and that are not easy to isolate (e.g. the effects of soil–structure interaction on the measured frequencies); (ii) the redundancy of the civil engineering structures, which results in low sensitivity of the method (i.e. small change of the overall stiffness and consequently of the measured frequencies) when the damage is localized; and (iii) the modeling uncertainties (if a model is used). Additional difficulties are: (iv) the uncertainties in the training data that might have been recorded under different conditions (if training data are used); (v) the completeness of the conceived damage scenarios and training data sets (if artificial neural networks are used); (vi) reliance on data from a larger number of sensors than usually available in structures (for the methods that monitor changes in mode shapes), and (vii) the measurement noise (see [1,2] for detailed state of the art reviews on this topic).

These factors are often collectively referred to as *noise*, and damage is detectable *only* if the changes it produces are larger than that noise. Hence, identifying and understanding *all* sources of noise is essential for a method to

*Corresponding author.
E-mail addresses: mtodorov@usc.edu (M.I. Todorovska), trifunac@usc.edu (M.D. Trifunac).

0267-7261/$ - see front matter © 2006 Elsevier Ltd. All rights reserved.
doi:10.1016/j.soildyn.2006.10.005

work on real life problems. This requires thorough understanding of *all* physical processes involved, besides the mathematical formalism of signal estimation in the presence of noise. Invaluable for understanding and proper treatment of the *actual* noise, and for validation of vibration based structural health monitoring methods are earthquake response data from well-instrumented full-scale structures that have been damaged by an earthquake. Unfortunately, such data are rare and not always available, and instead numerically simulated data are used for validation (see e.g. [3]). The numerically simulated data involve idealized models with stationary, zero mean, additive noise that is statistically independent of the structural response. The earthquake shaking and response of structures, however, are *not* stationary processes (especially not near the earthquake source where structural damage occurs most frequently), and the noise is not necessarily uncoupled from the signal. While simulation work is necessary in the early development stages, it does not guarantee that a method would work for real structures and real excitation. Less frequently, laboratory experimental data are also used to validate a method. While such physical tests are more realistic, in that they involve real materials, they also involve highly idealized modeling assumptions, both for the structure and for its boundary conditions. Real earthquake response data recorded in full-scale structures are rarely used, and often neglect important physical processes affecting the results (e.g. the effects of the soil).

A rare example of an instrumented building that has been damaged by an earthquake, and for which description of the damage and the strong motion data of the causative earthquake are available, is the former Imperial County Services (ICS) Building in El Centro, California, severely damaged by the magnitude 6.6 Imperial Valley earthquake of October 15, 1979, and later demolished [4]. Its transverse response was recorded by three vertical arrays, and its longitudinal response by one vertical array. As such, it makes an excellent benchmark problem to test structural health monitoring methods using real data.

The damage in this building was severe and obvious, while the challenge is to detect reliably smaller and hidden damage. Proving that a method is able to detect severe damage *does not imply* that it can detect less severe and hidden damage. However, being able to detect severe damage *is necessary* for a method to be able to detect less severe and hidden damage. While one can expect that any reasonably good method would be able to detect severe damage, analysis of such data can provide valuable information about the capabilities of a method and its sensitivity to noise in real data, beyond what can be learned from analysis of numerically simulated data. Some obvious advantages are as follows. The earthquake response data recorded in damaged full-scale structures involve realistic materials, boundary conditions, and excitation, each contributing to the realistic noise in the related estimation process. Comparison of the detected changes in the monitored parameters due to severe damage with realistic noise can help assess the limits of a method to detect less severe damage. Further, the capabilities of different methods in a real environment can be compared, which can help select directions for future research.

This paper is the first in a sequel of papers by the same authors on application of different structural health monitoring methods to this building, and a comparative analysis of their results. This paper deals with the most elementary approach—detecting changes in frequency estimated using some time–frequency distribution of the energy of the recorded response. Its objective is to introduce the case study for the sequel of papers (by presenting a description of the building, observed damage, and related strong motion data), and to present results using time–frequency analysis, to be used as a reference in the investigation of other methods. The particular time–-frequency analysis used is based on the Gabor transform [5], which, up to a phase shift, is equivalent to the moving window Fourier transform with a Gaussian window. For the purpose of completeness of this paper, the Gabor transform is briefly reviewed, including its close relationship to the moving window Fourier transform and the wavelet transform, and the reasons for choosing this transform. Artifacts in the estimation and the reliability of the results in different time intervals are also discussed. Results for the inter-story drifts estimated form the strong motion data are also shown, as independent characteristics of the response that are well correlated with damage. A comprehensive review of time–frequency analysis methods is out of the scope of this paper. It is only noted that these type of structural health monitoring methods are most wide spread of all vibrational methods because they require minimum instrumentation (e.g. one sensor at the roof, though an additional sensor at the base is preferable), and can be applied to most strong motion records in structures. It is also noted that, from among the difficulties mentioned in the first paragraph of this section, this method is most sensitive to (i), (ii), and (iv).

2. The case study

The former ICS Building was a six-story reinforced concrete structure located in the El Centro, California. It was designed in compliance with the 1967 Uniform Building Code, and its construction was completed in 1969. It had plan dimensions 41.70×26.02 m and height 25.48 m. Fig. 1 shows its foundation and ground floor (Fig. 1, top) and typical floor plan (Fig. 1, bottom). The foundation system had pile groups and the pile caps were directly located under the columns and walls. The pile caps were connected by ground-level beams. Up to depth of 9 m, the underlying soil consisted of soft to medium-stiff damp sandy clay with organic materials, with inter-layers of medium dense moist sand, and beneath 9 m it consisted of stiff, moist sandy clay and silty clay [4].

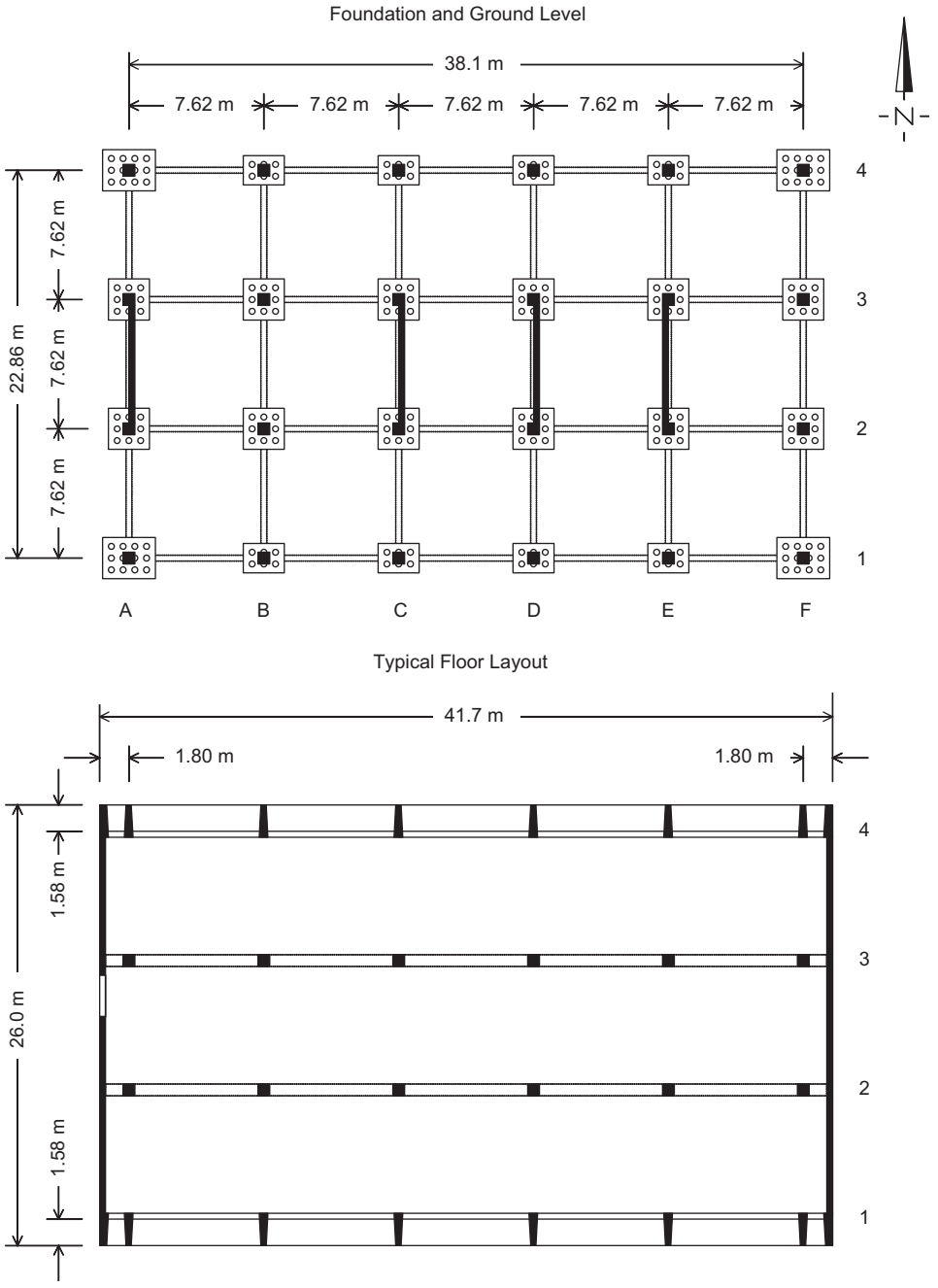

Fig. 1. Foundation and ground level plan (top) and typical floor layout (bottom) of the ICS building.

The structure was made of reinforced concrete, with minimum ultimate compressive strength of 27.6 MPa—for the walls, beams and slabs, 34.5 MPa—for the columns, and 20.7 MPa—for the foundation elements, with reinforcement steel of 276 MPa. The structural configuration in the NS (transverse) direction consisted of two concrete shear panels at the east and west ends of the building (see Fig. 1), which extended only from the second floor to the roof, and were supported by cantilever parts of the frame beams, which extended in the EW direction. At the ground level, four shear panels were located between axes 2 and 3 along lines A and C through E. In the EW (longitudinal) direction, the structural system consisted of four beam-column frames. The facade columns had a variable cross-section, varying from rectangular to trapezoidal at the second floor [4].

The 16-channel seismic monitoring array (installed by the California Geological Survey, formerly the California Division of Mines and Geology) consisted of a 13-channel structural array of force balance accelerometers (FBA-1), with a central analog recording system, and a tri-axial SMA-1 accelerometer in the "free field", approximately 104 m east from the northeast corner of the building. Fig. 2 shows the location and orientation of

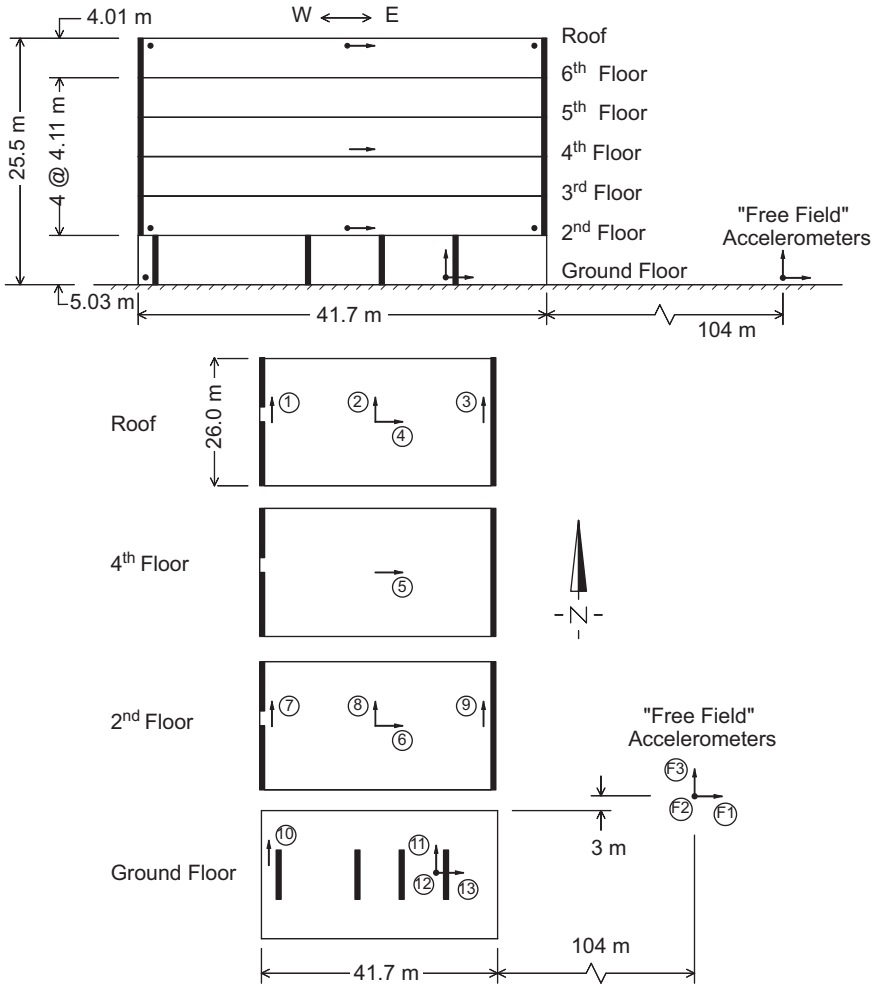

Fig. 2. Layout of the seismic monitoring array in the ICS building.

the sensors. The sensors for channels 1–4 were attached under the roof slab, and for 5–13—on the topside of the floor slabs. The recording system had a horizontal starter on the roof (adjacent and parallel to channel 4), and a vertical starter on the ground floor (adjacent to channels 11, 12 and 13). A more detailed description of the structural system and seismic instrumentation can be found in [4].

Ambient vibration tests of the building were conducted several months prior the earthquake, on February 26 and 27, and on May 17, 1979 [6]. Unfortunately, these involved only measurements at the second, fourth, sixth and seventh story (roof), without a reference site on the ground floor, which is necessary to compute the transfer-functions between structural response and ground motion, and eliminate the effects of site frequencies. EW motion spectra, recorded at each of the mentioned floors along the west side of the building (near the center of the west outer wall), showed a peak near 1.54 Hz, which was interpreted as the EW building frequency. The NS motions were recorded at the same locations along the west wall (near the center of the west outer wall), and also along the center of the north outer wall of the building. The spectra of the former had a peak near 2.81 Hz, which was interpreted as the torsional frequency, and of the latter had a peak near 2.24 Hz, which was interpreted as the NS building frequency. The interpretation of the torsional frequency was based on the change of phase of the recorded absolute motions. Simultaneous measurement of NS motions along the west and east ends of the building would have enabled more reliable estimation of the torsional frequency.

The Imperial Valley earthquake of October 15, 1979 ($M_L = 6.6$, depth $H = 8$ km) occurred on the Imperial Fault near El Centro, California, at epicental distance of about 26 km southeast from the building (Fig. 3). From the hypocenter, the dislocation propagated northwest with velocity near 2.5 km/s, and after about 9 s it passed by the closest distance to the building, 7 km to southwest (Fig. 3; [7,8]). Thus, during the first 9 s, the building was receiving larger than average power of strong motion, due to strong source directivity towards northwest.

The building was severely damaged by this earthquake, and was later demolished [4]. Fig. 4 shows a schematic

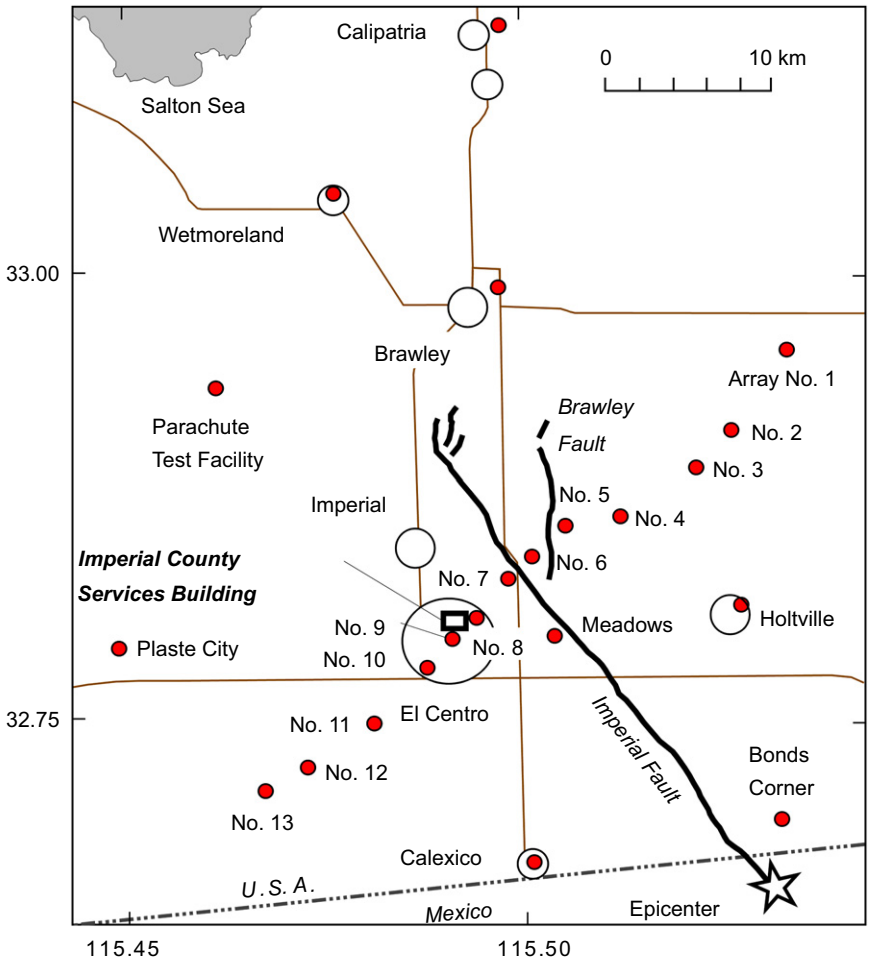

Fig. 3. Location of the Imperial Fault relative to the ICS building site and strong motion stations in Imperial Valley in 1979.

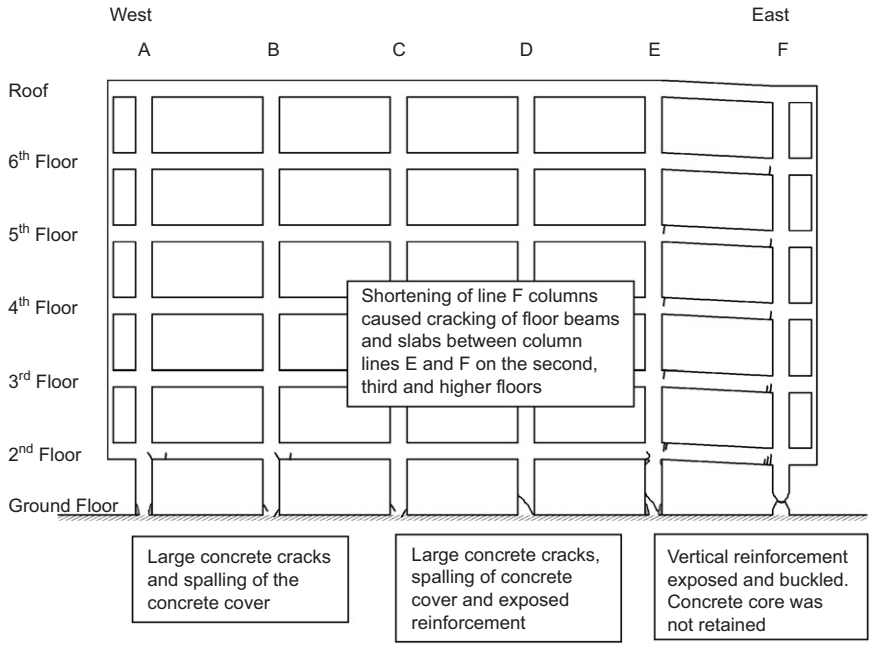

Fig. 4. Schematic representation of the damage in the ICS building following the 1979 Imperial Valley earthquake (reproduced from [4]).

representation of the observed damage. The major failure occurred in the columns of frame F (at the east end of the building) at the ground floor. The vertical reinforcement was exposed and buckled, and the core concrete could not be contained, resulting in sudden failure and shortening of the columns subjected to excessive axial loads. This in turn caused an incipient vertical fall of the eastern end of the building, causing cracking of the floor beams and slabs near column line F on the second, third and higher floors. Columns in lines A, B, D and E also suffered damage. Columns in frames A and E did not suffer as extensive damage as shortening and buckling of the reinforcement in line F at the east side, but large concrete cracks and exposed reinforcement could be seen near the base. In the columns in interior frames B–E, visible cracks and spalling of the concrete cover were also observed [4].

All 16 channels recorded the earthquake. The recorded peak accelerations at the roof and ground floor were 571 and 339 cm/s^2 in the NS direction and 461 and 331 cm/s^2 in the EW direction. The film records were digitized by Trifunac and processed at USC [9]. The data released was sampled at 0.02 s, and band pass filtered between 0.1–0.125 and 25–27 Hz.Fig. 5 shows the corrected accelerations (part (a)), and the displacements obtained by (double) integration of the corrected accelerations (part (b)). The low frequency cut-off is determined so that the (signal + noise) amplitude is greater than the amplitude of noise due to a "wavy" baseline of accelograms recorded on film. Hence, the displacements shown in Fig. 5b do not contain the long period components below the cut-off frequency, including the static component. The implications on the computed inter-story drifts are discussed in the Results and analysis section.

3. Methodology

The Gabor transform [5] is a complex-valued time–frequency distribution, which represents a projection of the signal onto a family of Gabor wavelets, which are complex exponentials of circular frequency ω, modulated by a Gaussian envelope, and shifted relative to each other. Let $g_{(b,\omega)}(t)$ be a Gabor wavelet with frequency ω and centered at time b, and let $\hat{g}_{(b,\omega)}(\xi)$ be its Fourier transform. The Gabor wavelet can be written as

$$g_{(b,\omega)}(t) = g(t-b)\,\exp[\mathrm{i}\omega(t-b)], \tag{1}$$

where b is time, ω is circular frequency, and

$$g(t) = \pi^{1/4}\,\exp\left[-\frac{t^2}{2\sigma^2}\right] \tag{2}$$

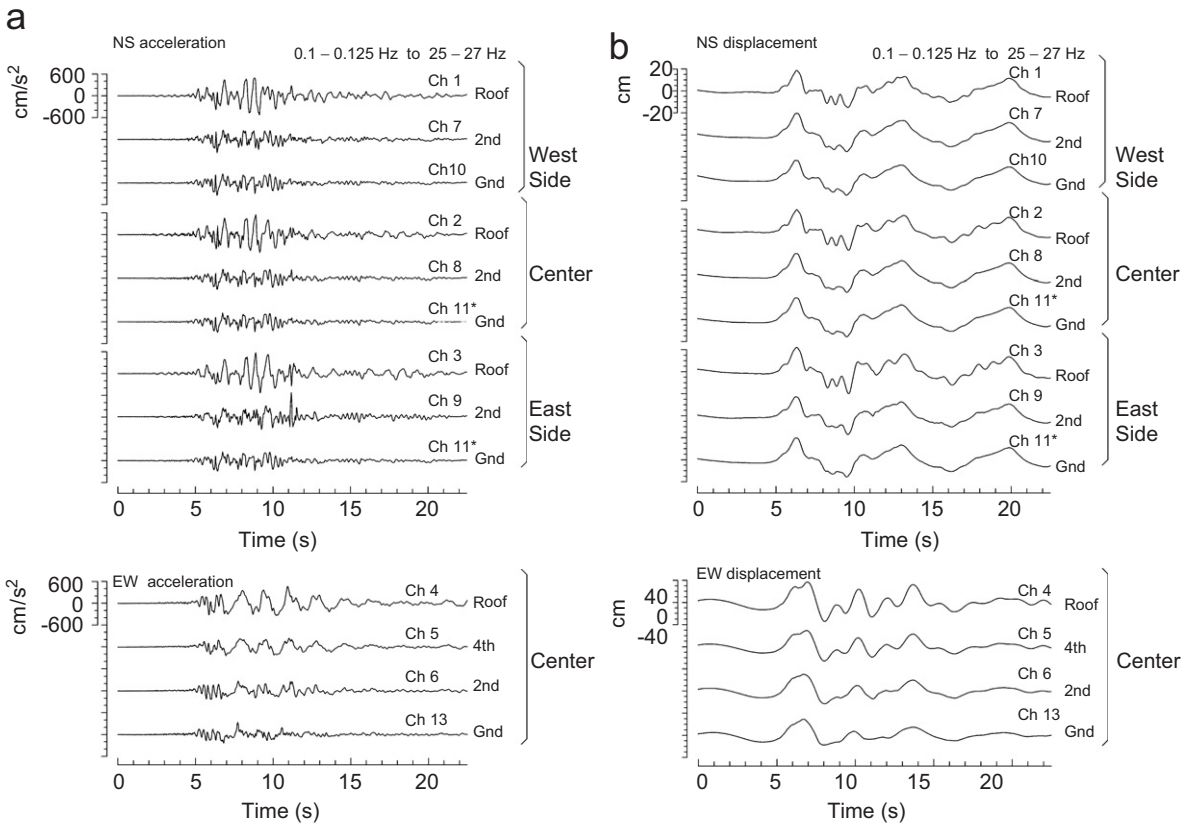

Fig. 5. (a) NS and EW components of accelerations recorded in the ICS building during the 1979 Imperial Valley earthquake, and (b) displacements obtained by integration.

is a Gaussian window symmetric about the origin. The Gabor transform of a signal $f(t) \in L_2(R)$ is by definition

$$G_f(b,\omega) \triangleq \int_{-\infty}^{\infty} f(t)\bar{g}_{(b,\omega)}(t)\,\mathrm{d}t, \quad \infty < b < \infty, \quad |\omega| > 0, \tag{3}$$

where ω is circular frequency. By the Parseval relation, it can also be computed in the frequency domain from the Fourier transforms of f and g

$$G_f(b,\omega) = \frac{1}{2\pi}\int_{-\infty}^{\infty} \hat{f}(\xi)\bar{\hat{g}}_{(b,\omega)}(\xi)\,\mathrm{d}t, \quad \infty < b < \infty, \quad |\omega| > 0, \tag{4}$$

where

$$\hat{g}_{(b,\omega)}(\xi) = \frac{1}{2\pi}\int_{-\infty}^{\infty} g_{(b,\omega)}(t)\,\mathrm{e}^{-\mathrm{i}\xi t}\,\mathrm{d}t = \pi^{1/4}\sqrt{2\pi\sigma}\,\exp[-\mathrm{i}\xi b]\,\exp\left[-\frac{1}{2}(\xi-\omega)^2\sigma^2\right] \tag{5}$$

is the Fourier transform of the Gabor wavelet. From Eq. (4), the Gabor transform can also be interpreted as the projection of the Fourier transform of the function onto the Fourier transform of the wavelet.

The instantaneous system frequency was determined from the *ridge* of the Gabor transform of the relative horizontal roof displacement with respect to that of the ground floor. The ridge is the collocation of points on the time–frequency plane where the magnitude of the transform (i.e. the energy of the signal) is maximal. The value of the magnitude of the transform along the ridge is called skeleton, and is a smooth estimate of the amplitude envelope of the signal. From the ridge and skeleton alone, an approximation of the original signal can be reconstructed.

For a simplified soil–structure interaction model of a building supported by a rigid foundation, the difference between the roof and base horizontal displacements is the sum of the horizontal displacements due to rigid body rocking of the foundation and due to deformation of the structure. The estimated frequency from such data is referred to as system or "apparent" building frequency, which differs from the fixed-base frequency. While the fixed-base frequency depends only on the properties of the structure, the apparent frequency depends also on the stiffness of the foundation soil. The following relationship holds [10]

$$\frac{1}{\omega_{\mathrm{sys}}^2} = \frac{1}{\omega_1^2} + \frac{1}{\omega_{\mathrm{H}}^2} + \frac{1}{\omega_{\mathrm{R}}^2}, \tag{6}$$

where ω_{sys} is the soil–structure system frequency, ω_1 is the fundamental fixed-base frequency of the structure, and ω_{H} and ω_{R} are the horizontal and rocking frequencies of a rigid structure on flexible soil.

The Gabor transform is closely related to a moving window analysis (also called "short time Fourier transform", or "windowed Fourier transform"), commonly used to estimate variations of the building frequency with time during the earthquake shaking during the past 30 years [11]. The major difference between the two is that, while *any* window function can be used for the windowed Fourier transform, the most common one being a tapered box function, the Gabor transform is defined *only* for a Gaussian window, which has the best combined time and frequency resolution of all possible window functions, and is therefore optimal [12]. If the windowed Fourier transform uses a Gaussian window $g(t)$ [13], same as in Eq. (2), then it is *identical* to the Gabor transform up to a phase shift. For example, if $\mathrm{WFT}_f(b,\omega)$ is the windowed Fourier transform of a function $f(t)$

$$\mathrm{WFT}_f(b,\omega) = \int_{-\infty}^{\infty} f(t)g(t-b)\,\exp[-\mathrm{i}\omega t]\,\mathrm{d}t \tag{7}$$

it can be easily shown that

$$G_f(b,\omega) = \mathrm{WFT}_f(b,\omega)\,\exp[\mathrm{i}\omega b]. \tag{8}$$

As the difference between the two transforms is only in phase shift, while their magnitude—hence ridge—are the same, both transforms will give identical results for the instantaneous frequency provided that the shape of the window is exactly the same.

The Gabor transform is also related to the complex wavelet transform using a Morlet wavelet, which is essentially a Gabor transform with a variable length time window enclosing equal number of cycles at all frequencies (see e.g. [14]. Consequently, the Gabor transform has the same resolution at all frequencies. The wavelet transform has better time resolution at high frequencies, at the expense of lowering the frequency resolution, which is inevitable as per the Heisenberg–Gabor principle of uncertainty, which states that the product of the time and frequency uncertainties is always constant for a given window, and is the smallest for the Gaussian window.

For ideal asymptotic signals, which are signals whose amplitude envelope changes slowly with time, compared to the change in phase, and for comparable window sizes the Gabor transform and the wavelet transform yield very similar results for the instantaneous frequency of structures. For the analysis of *real* earthquake data recorded in full-scale structures, such as in this paper, the authors prefer to use the Gabor transform, which has a *constant width* window, because it enables better control of the frequency resolution at higher frequencies, i.e. at the beginning of shaking, when the amplitude envelope is small and rapidly grows with time (violating the asymptoticity assumption on which the method for estimation of instantaneous frequency is based), while the system frequency rapidly decreases with time. In this time interval, the signal (structural response) is weak, as it takes time for the first mode of vibration to be fully excited (after which it dominates the response), and is contaminated by noise.

The noise is due to the fact that the excitation is not white noise, and due to a "wavy" baseline (long period noise), which is mostly removed by digitization of a fixed baseline and high pass filtering [15]. The long period noise leads to low estimates of the system frequency in the beginning of the record, which appear to be artifacts, and are therefore not shown. To abate this problem, it is convenient to high pass filter the record (for estimation of the early changes in frequency only), and to use a wavelet with a narrow enough Fourier transform. An advantage of using a variable time window is that once σ is chosen appropriately, one does not have to worry that the window may be too short and does not contain sufficient number of cycles for a meaningful estimation. However, for civil structures, the changes in frequency are within an order of magnitude, and are viewed on a linear frequency axis, so that a variable window is not necessary. A variable window transform would be more appropriate for processes where the frequency is viewed on a logarithmic scale.

For the case study in this paper, $\sigma = 1$ s was used (see Eq. (2)), which implies resolution in time and in linear frequency, $\nu = \omega/2\pi$, $\sigma_t = (1/\sqrt{2})\sigma = 0.71$ s and $\sigma_\nu = (1/2\pi)(1/\sqrt{2})(1/\sigma) = 0.11$ Hz [14]. Hence, the meaning of "instantaneous" frequency $\nu(t)$ is that, within the time interval $t \pm \sigma_t$, the frequency is within the interval $\nu \pm \sigma_\nu$. Another important fact in the interpretation of the results by this method is the assumption of asymptoticity—that the envelope of the signal changes very slowly within one period, and hence, the time variation of the signal is mostly due to change in phase. When this condition is violated, the method gives sharp variations of the frequency that are artifacts. A longer window of the Gabor wavelet (larger σ) generally smoothes such variations.

4. Results and analysis

4.1. Drifts and Fourier spectra

Fig. 6 shows the NS (top) and EW (bottom) inter-story drifts computed from the displacements shown in Fig. 5b. The horizontal lines show 0.5%, 1% and 1.5% drift levels. Because these drifts were computed from band-pass filtered data, they do not represent the actual drifts but their limited view—through a tapered window in the frequency

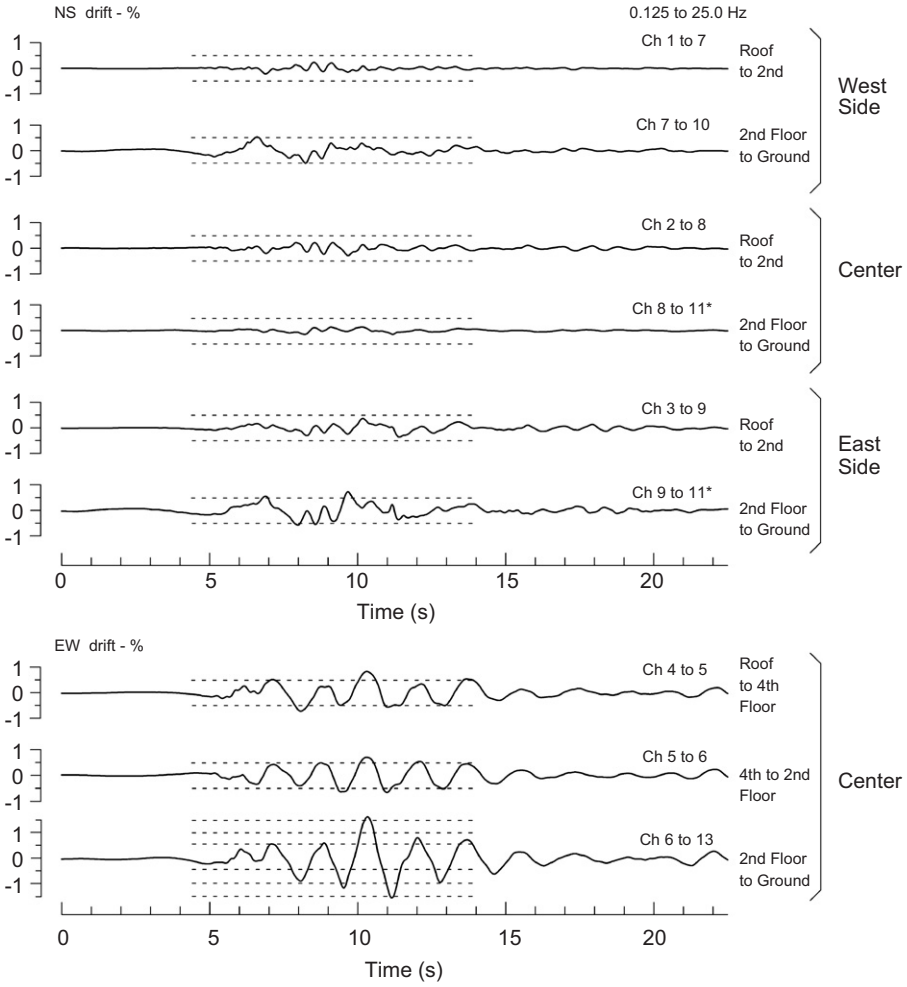

Fig. 6. Inter-story drifts recorded in the ICS building during the 1979 Imperial Valley earthquake. The horizontal lines mark 0.5%, 1% and 1.5% drift levels.

domain (between 0.1–0.125 and 25–27 Hz). As a result of the high-pass filtering, these drifts do not contain any contributions from permanent deformation, e.g. due to damage or due to permanent rotation of the foundation. Also, these drifts represent the sum of the drift due to *rigid body rocking* (one of the effects of soil–structure interaction) and drift due to relative *deformation* of the building, which could not be separated because of inadequate instrumentation. Hence, the computed "windowed" drifts can be considered as lower bounds of the actual *total* drifts (due to deformation of the structure and foundation rocking), and as upper bounds of the "windowed" drifts due to deformation of the structure. The latter judgment is based on the assumption that the fundamental NS and EW modes of vibration contribute most to the response, these drifts can be considered as upper bounds of the actual drifts due to deformation of the structure, as near the first system frequencies the relative response due to deformation of the structure is generally in phase with the foundation rocking [16]. Their actual values, hence, have to be interpreted with caution. In what follows, the windowed total drifts will be referred to simply as "drifts", and are considered as some approximate *measures* for the actual drifts due to deformation of the structure.

These drifts in Fig. 6 suggest: (1) "soft" first story in both NS and EW directions, and (2) larger flexibility in the EW direction. In the EW direction, the drift exceeded 1.5%, and in the NS direction it exceeded 0.5%. The first story drifts are significantly larger at the ends than at the center of the building, suggesting (3) significant torsional response, probably amplified by the wave passage, and by the asymmetric distribution of stiffness in the NS direction at the soft first story (see Figs. 1 and 2). The first story drifts are larger at the east side, initially as a result of the smaller stiffness at that end, and later due to the larger damage.

Fig. 7 shows Fourier spectra for the NS (left) and EW (right) ground floor accelerations (top), and relative displacements (bottom), all at the center of the building. (The NS ground motion at the center of the building was estimated by interpolation using data from channels 10 and 11, and the roof motion is that recorded by channel 2). The roof spectra suggest a wide variation of the NS system frequency (0.7 to about 2 Hz), and EW system frequency near 0.6 Hz during most of the duration of shaking. The thick lines show the apparent frequencies as interpreted from ambient vibration tests data (1.54 Hz for EW motions, 2.24 for NS motions, and 2.81 for torsion; [6]).

4.2. Observed changes of frequency

Figs. 8 and 9 show the "instantaneous" system frequency from the ridge of the Gabor transform of the roof relative response with $\sigma = 1$, respectively, for NS and for EW motions, and show the variations of frequency with time and amplitude of response. The results were computed using FORTRAN program `inst_frq` [14].

Parts (a) and (b) show the ground floor accelerations, and the roof relative displacements (at the center of the building), both included as background information. Part (c) shows the skeleton (the thicker line), which is a smoothed estimate of the amplitude envelope of the estimated signal, which is the relative roof response near the first system frequency. The thin line is the actual amplitude envelope (that for the broad-band signal), determined by Hilbert transform [14]. This plot is included to help monitor rapid changes in the amplitude of the signal and artifacts in the estimate of instantaneous frequency caused by violations of the asymptoticity condition. Part (d) shows the Fourier spectra of the relative roof displacement (the solid line), and of the ground floor acceleration (the dashed line, on a relative scale), both included as background information. Part (e) shows the variations of the system frequency as function of amplitude of response (estimated from the ridge and

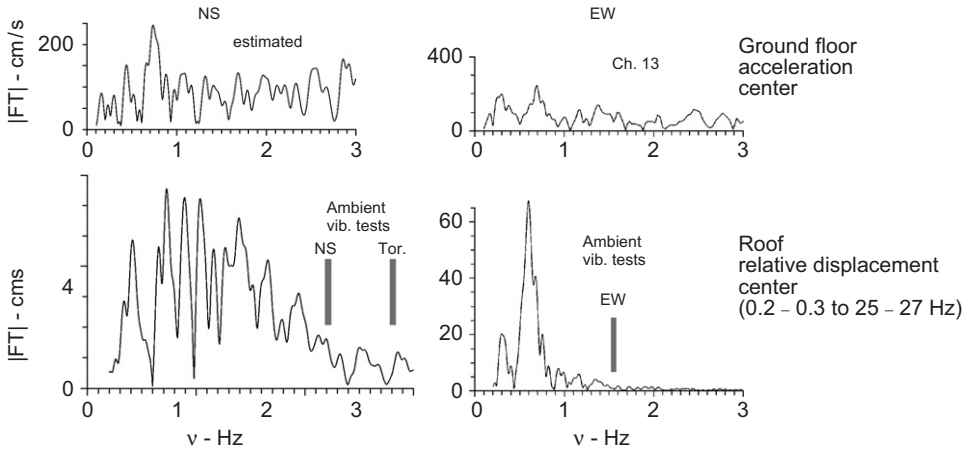

Fig. 7. Fourier transform amplitudes of NS (left) and EW (right) ground floor acceleration (top), and relative displacement (bottom), at the center of the ICS building during the 1979 Imperial Valley earthquake. The thick lines show the EW, NS and torsional frequencies reported from ambient vibration tests prior to the earthquake [6].

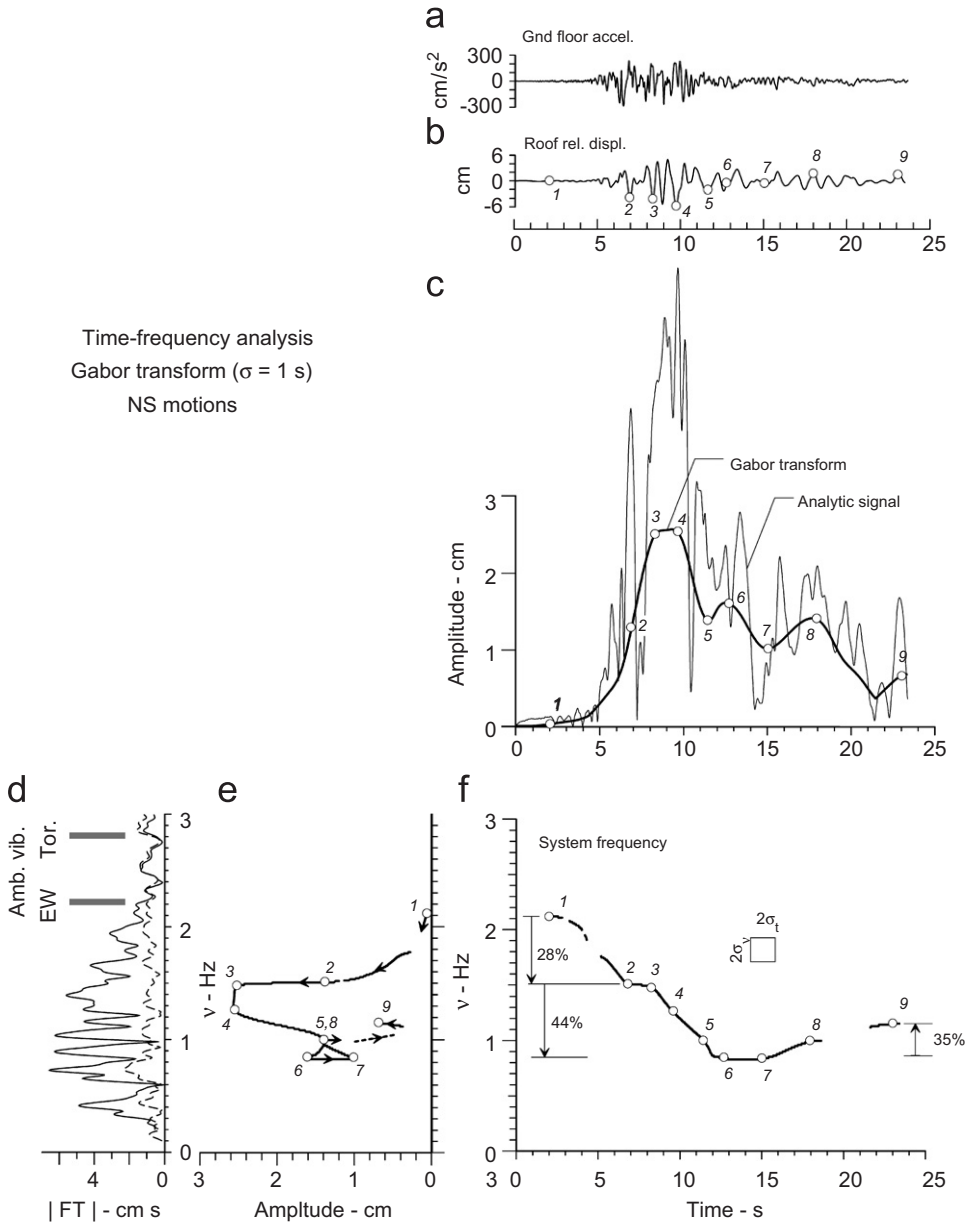

Fig. 8. Time–frequency analysis for the NS response of the ICS building: (a) ground acceleration, (b) relative response, (c) amplitude envelope, (d) Fourier spectrum of relative response (solid line) and of ground acceleration (dashed line, (e) amplitude of relative response versus frequency, (f) system frequency versus time.

skeleton of the Gabor transform), with the arrows indicating the direction of increasing time. Part (f) shows the variations of the system frequency versus time, estimated from the ridge of the Gabor transform. The output of computer program `inst_frq` also produces the instantaneous frequency estimate using Hilbert transform, but these estimates are not shown in Figs. 8 and 9 as they are "noisy" and obstruct the physical analysis of the results. The missing segments and the dashed lines in parts (e) and (f) correspond to time intervals where the estimates cannot be obtained or are not believed to be reliable, due to rapid variations of the envelope of the amplitude, and/or very weak "signal". The rectangle in part (f) with sides $2\sigma_t = 1.42$ s and $2\sigma_\nu = 0.22$ Hz illustrates the theoretical uncertainty of the estimates due to the finite resolution of the Gabor transform. In practice, the uncertainty is larger due to violations of the asymptoticity assumption. Finally, the numbered open dots (occurring at different times in parts (b), (c) (e) and (f)) correspond to some characteristic points in time associated with changes in amplitude or frequency, as well as few other points in-between.

Fig. 8, part (f), shows that the NS frequency dropped from $\nu \approx 2.12$ Hz in the early stage of response (at $t \approx 2$ s) to $\nu \approx 1.52$ Hz at $t \approx 6.8$ s ($\Delta\nu \approx 0.6\,\text{Hz} > \sigma_\nu$, $\Delta\nu/\nu \approx 28\%$),

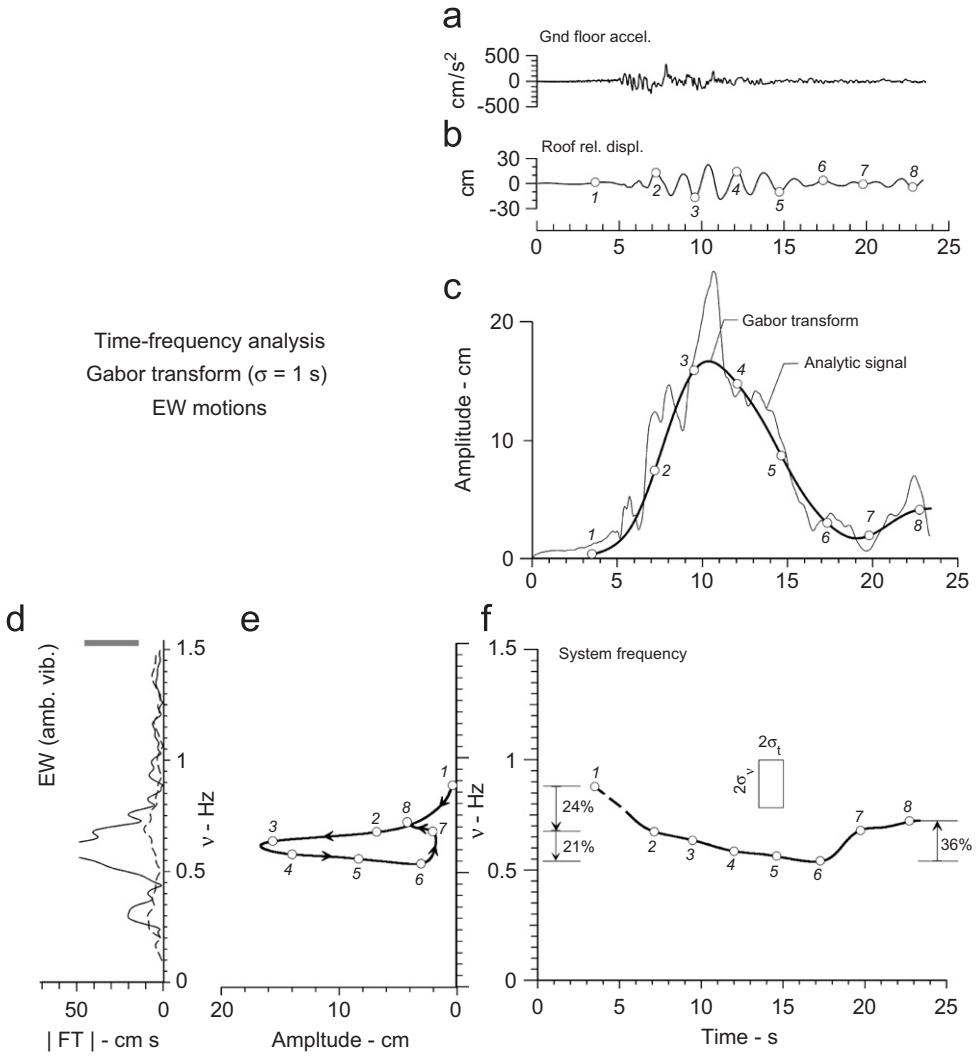

Fig. 9. Same as Fig. 8 but for the EW response.

was constant in the interval $t \approx 6.8$–8.5 s, and further dropped to $\nu \approx 0.85$ Hz at $t \approx 12$ s ($\Delta\nu \approx 0.67$ Hz $> \sigma_\nu$; $\Delta\nu/\nu \approx 44\%$). Then, towards the end of the recorded shaking, the frequency increased to $\nu \approx 1.15$ Hz ($\Delta\nu \approx 0.3$ Hz; $\Delta\nu/\nu \approx 35\%$).

Fig. 9, part (f), suggests that the EW frequency dropped rapidly from $\nu \approx 0.88$ Hz at $t \approx 3.5$ s to $\nu \approx 0.67$ Hz at $t \approx 7$ s ($\Delta\nu \approx 0.21$ Hz $> \sigma_\nu$; $\Delta\nu/\nu \approx 24\%$), and then continued to drop gradually to $\nu \approx 0.53$ Hz at $t \approx 17$ s ($\Delta\nu \approx 0.14$ Hz $\approx \sigma_\nu$; $\Delta\nu/\nu \approx 20.9\%$). Similarly as for the NS response, the frequency increased to about 0.72 Hz at the end of the record ($\Delta\nu \approx 0.19$ Hz; $\Delta\nu/\nu \approx 36\%$).

Parts (e) of Figs. 8 and 9 show initial rapid decrease of frequency with amplitude of response (between points 1 and 2) in the beginning of shaking, followed by a slower rate of decrease as the amplitudes of motion increased to their maximum values (between points 2 and 3), a rapid decrease during the largest amplitudes of response (between points 3 and 4), and further decrease as the amplitude of motion decreased (between points 4 and 6). Both frequencies started to increase near the end of the record, regardless of the trend of the (small) amplitudes of response.

5. Discussion

The major damage occurred in the first story columns at the east side of the building. Fig. 6 shows that both the NS and EW first story drifts were below 0.5% until $t \approx 7$ s. The NS first story drifts at that east side were the largest between $t \approx 9.5$ and 10 s, exceeding 0.5%. Within the same time interval, the EW first story drifts exceeded 1%, reaching and exceeding 1.5% shortly after $t = 10$ s, and again shortly after $t = 11$ s in the next half of the cycle. This suggests that the observed drops of system frequency that occurred before $t \approx 7$ s (of about 28% for NS and 24% for EW motions, between points 1 and 2 in parts (f) of Figs. 8 and 9), were likely not caused by severe structural damage. The following drop of system frequency, of about 44% for

NS motions and 21% for EW motions (between points 2 and 6) were most likely due to damage.

The degree to which different factors have contributed to the initial decrease of the system frequency in this building cannot be determined with certainty with the data available. One of the possible contributors is degradation of structural stiffness caused by non-structural damage, and by smaller or even invisible structural damage. For example, Zembaty et al. [17] report about 10% reduction of the frequency of an RC frame, testes on a shake table, before any cracks in the concrete could be detected. Another possible contributor is change in the foundation system, such as formation of gaps between the foundation and the soil (geometric non-linearity), and softening (yielding) of the soil (material non-linearity), which has been observed, e.g. in geotechnical experiments of pile foundations and in field investigations. The formation of gaps results in lowering of the effective point of fixity of the building, leading to larger effective height and smaller fundamental fixed-base frequency (ω_1 in Eq. (6)), while the softening of the soil leads to smaller frequencies ω_H and ω_R in Eq. (6). Such hypothesis was used by Trifunac et al. [18,19] to explain the system frequency variations of a seven-story RC hotel in Van Nuys, in the Los Angeles metropolitan area, damaged by the 1994 Northridge earthquake. The extent of such non-linear effects in the foundation system depends on how soft the underlying soil is. At the site of the ICS building, the underlying soil, up to depth of 9 m, consists of soft to medium-stiff damp sandy clay with organic materials, with inter-layers of medium dense moist sand, and beneath 9 m—of stiff, moist sandy clay and silty clay [4]. Consequently, such non-linear effects were possible.

It should be mentioned here that repeated earthquake recordings in buildings have revealed variability of their system frequency, as function of the amplitude of shaking and time, during a particular earthquake and from one earthquake to another. Some of the observed changes are permanent and some are temporary. For example, temporary changes (recovery after the earthquake, during aftershock shaking), as large as 20% for some buildings, have been reported by Todorovska et al. [20] based on a study of 21 buildings in the Los Angeles area that recorded 1994 Northridge earthquake and aftershocks. For Millikan Library in Pasadena, California, which has been monitored over a period of 36 years [21], both permanent (long term trend of reduction over time of 22% for EW and 12% for NS response, most of which occurred during the 1971 San Fernando earthquake), and temporary changes (well correlated with the amplitude of shaking) of the building frequency during earthquakes have been reported, while there has been no reported significant structural damage. Moreover, Clinton et al. [21] report short term changes correlated with the local weather (strong wind, heavy rainfall, and very hot weather) of the order of several percent, based on analysis of continuously recorded response at the roof over a period of several years. Todorovska and AlRjoub [22] showed that the variations with heavy rainfall can be explained by a soil–structure interaction model based on Biot's theory of wave propagation in fully saturated porous soils. Similar variability of the building frequency from one event to another has been observed for other buildings, e.g. one in Iceland [23] and another one in Japan [24]. The latter has been well instrumented for soil–structure interaction analyses, and the trend of decreasing building frequency with time has been attributed to degradation of stiffness in the building. For the ISC building, only records of the Imperial Valley earthquake are available. Hence, it is not possible to tell whether and to which degree the observed initial change in frequency would have been recoverable.

Finally, increase of the system frequency following the strongest shaking, (indicating system hardening) has been also observed for other buildings subjected to damaging ground shaking, e.g. the seven-story RC hotel in Van Nuys during the M_L 6.4 Northridge earthquake in 1994 [19], and for a four-story RC building in Bonefro, Italy, during a M 5.3 event of the 2002 seismic sequence in Molise [25].

6. Summary and conclusions

The ICS Building had a soft first story, with non-symmetric distribution of stiffness in the first story, which was smaller at the east end of the building. Consequently, torsion contributed significantly to the response, and the inter-story drifts were the largest in the first story columns at the east side of the building, as confirmed by the strong motion data. Not surprisingly, the most severe damage occurred in the first story columns at the east end of the building. The data shows that the EW (longitudinal) inter-story drifts exceeded 1.5% in the first story. The NS (transverse) drifts were smaller (due to the larger stiffness) but exceeded 0.5% in the first story. It is noted that these are windowed (in frequency) total drifts, which include contributions both from foundation rocking and from deformation of the structure.

The (first) system frequencies and amplitudes of relative response were estimated from the ridges and skeletons of the Gabor transform of the relative roof horizontal displacement. The Gabor transform was preferred to the wavelet transform because of better control over the frequency resolution during the early stage of response, where the system frequency is the largest, and the signal-to-noise ratio is small. The earliest estimates of system frequency could be obtained at $t \approx 2$ s for NS motions and at $t \approx 3.5$ s for EW motions, but those for $t > 5$ s are most reliable. For both components of motion, early in the response ($t < 7$ s), a decrease of system frequency was detected of about 28% for NS and 24% for EW motions. During this time, the amplitudes of the first story drifts were relatively small ($< 0.5\%$), and the decrease is believed to be due to changes in the soil and bonding between the soil and foundation. This was followed by a further decrease of the system frequency, of about 44% for NS

(between 8 and 12 s) and 21% for EW motions (between 7 and 17 s). The first story drifts were large when this occurred ($>0.5\%$ for NS and $>1.5\%$ for EW motions) and the principal cause for this change is believed to be the damage. The most severe damage occurred between 8 and 12 s after trigger. Near the end of shaking, an increase of system frequency was observed, 35% for NS and 36% for EW motions, suggesting system hardening. It is noted here that the mentioned percentage changes are not expressed with respect to an absolute reference value, but with respect to a relative reference, which is the *previous* value for each particular change quoted. The system frequencies reported from ambient vibration tests (2.24 Hz for NS vibrations, and 1.54 Hz for EW vibrations; [6]) are much higher than those observed during the earthquake, and cannot be used as a baseline in detecting the time or state of damage in this building.

The next paper in the sequel [26] presents and analysis of novelties in the recorded accelerations detected using biorthogonal wavelets, used as indicators of the occurrence of damage.

Acknowledgements

The software used for the analysis in this paper was developed as part of a project supported by the National Science Foundation under Grant No. CMS-0075070 (PI: M. Todorovska). Any opinions, findings, and conclusions or recommendations expressed in this paper are those of the authors and do not necessarily reflect the views of the National Science Foundation.

References

[1] Chang PC, Flatau A, Liu SC. Review paper: health monitoring of civil infrastructure. Struct Health Monit 2003;2(3):257–67.
[2] Doebling SW, Farrar CR, Prime MB, Shevitz DW. Damage identification and health monitoring of structural and mechanical systems from changes in their vibration characteristics: a literature review. Report LA-13070-MS, Los Alamos National Laboratory, Los Alamos, NM; 1996.
[3] Johnson EA, Lam HF, Katafygiotis LS, Beck JL. Phase I IASC-ASCE structural health monitoring benchmark problem using simulated data. J Eng Mech ASCE 2004;130(1):3–15.
[4] Kojić S, Trifunac MD, Anderson JC. A post earthquake response analysis of the Imperial County Services building in El Centro. Report CE 84-02, University of Southern California, Department of Civil Engineering, Los Angeles, CA; 1984.
[5] Gabor D. Theory of communication. J Inst Elect Eng 1946;93:429–57.
[6] Pardoen GC. Ambient vibration tests results of the Imperial County Services Building. Bull Seism Soc Amer 1983;73(6):1895–902.
[7] Jordanovski LR, Trifunac MD. Least square model with spatial expansion: application to the inversion of earthquake source mechanism. Soil Dynam Earthquake Eng 1990;9(6):279–83.
[8] Jordanovski LR, Trifunac MD. Least square inversion with time shift optimization and an application to earthquake source mechanism. Soil Dynam Earthquake Eng 1990;9(5):243–54.
[9] Trifunac MD, Lee VW. Automatic digitization and processing of strong motion accelerograms. Parts I and II, Department of Civil Engineering, Report No. 79-15, University of Southern California, Los Angeles, California; 1979.
[10] Luco JE, Wong HL, Trifunac MD. Soil–structure interaction effects on forced vibration tests. Department of Civil Engineering, Report No. 86-05, University of Southern California, Los Angeles, CA; 1986.
[11] Udwadia FE, Trifunac MD. Time and amplitude dependent response of structures. Earthquake Eng Struct Dynam 1974;2: 359–78.
[12] Carmona R, Hwang WL, Torresani B. Practical time–frequency analysis: Gabor and wavelet transforms with an implementation in S. New York: Academic Press; 1998.
[13] Mark WD. Spectral analysis of convolution and filtering of non-stationary stochastic processes. J Sound Vib 1970;11(1):19–63.
[14] Todorovska MI. Estimation of instantaneous frequency of signals using the continuous wavelet transform. Report CE 01-07, Department of Civil Engineering, University of Southern California, Los Angeles, California; 2001. p. 55.
[15] Trifunac MD, Udwadia FE, Brady AG. Analysis of errors in digitized strong motion accelerograms. Bull Seism Soc Amer 1973;63(1):157–87.
[16] Todorovska MI, Trifunac MD. The system damping, the system frequency and the system response peak amplitudes during in-plane building-soil interaction. Earthquake Eng Struct Dyn 1992;21(2): 127–44.
[17] Zembaty Z, Kowalski M, Pospisil S. Dynamic identification of a reinforced concrete frame in progressive states of damage. Eng Struct 2006;28(5):668–81.
[18] Trifunac MD, Ivanović SS, Todorovska MI. Apparent periods of a building I: Fourier analysis. J Struct Eng ASCE 2001;127(5): 517–26.
[19] Trifunac MD, Ivanović SS, Todorovska MI. Apparent periods of a building II: time–frequency analysis. J Struct Eng ASCE 2001;127(5):527–37.
[20] Todorovska MI, Trifunac MD, Hao TY. Variations of apparent building frequencies—lessons from full-scale earthquake observations. In: Proceedings of the first european conference on earthquake engineering and seismology, Geneva, Switzerland, 3–8 September 2006, Paper Number: 1547; 2006. p. 9.
[21] Clinton JF, Bradford SK, Heaton TH, Favela J. The observed wander of the natural frequencies in a structure. Bull Seism Soc Amer 2006;96(1):237–57.
[22] Todorovska MI, Al Rjoub Y. Effects of rainfall on soil–structure system frequency: examples based on poroelasticity and a comparison with full-scale measurements. Soil Dynam Earthquake Eng 2006;26(6–7):708–17.
[23] Snæbjörnsson Jt, Sigbjörnsson R. Monitoring the dynamics of a concrete building enduring earthquake and wind excitation. In: Proceedings of the first european conference on earthquake engineering and seismology, Geneva, Switzerland, 3–8 September 2006, Paper Number: 1207; 2006. p. 10.
[24] Kashima T, Kitagawa Y. Dynamic characteristics of an 8-storey building estimated from strong motion records. In: Proceedings of the first european conference on earthquake engineering and seismology, Geneva, Switzerland, 3–8 September 2006, Paper Number: 1005; 2006. p. 10.
[25] Mucciarelli M, Masi A, Gallipoli MS, Harabaglia P, Vona M, Ponzo F, Dolce. Analysis of RC building dynamic response and soil-building resonance based on data recorded during a damaging earthquake (Molise, Italy, 2002). Bull Seism Soc Am 2004;94(5): 1943–53.
[26] Todorovska MI, Trifunac MD. Earthquake damage detection in the Imperial County Services Building II: analysis of novelties via wavelets. Soil Dynam Earthquake Eng 2006, submitted for publication.